Nonlinear Pattern Selection in Binary Mixture Convection with Through-Flow

Guo-Dong Li[1,3], Atsushi Ogawa[2], Yoshifumi Harada[2], and Michael I.Tribelsky[1]
[1]*Department of Applied Physics,* [2]*Department of Human and Artificial Intelligent Systems, Faculty of Engineering, Fukui University, Bunkyo 3-9-1, Fukui 910-8507, Japan*
[3]*Institute for Fluid Dynamics, Xi'An University of Technology, Xi'An 710048, China*
(February 8, 2008)

Abstract

The pattern selection problem in binary-mixture convection in an extended channel with a lateral through-flow is presented. The through-flow breaks left–right parity and changes pattern dynamics dramatically. The problem is studied based on computer simulation of the complete set of hydrodynamic equations (Oberbeck-Boussinesq approximation) in the two-dimensional rectangular channel with aspect ratio $\Gamma = 12$ and convection-suppressing lateral boundary conditions. A wide variety of new dynamical patterns is obtained, discussed and classified.

PACS numbers: 47.20.Ky, 47.27.Te, 47.54.+r

Convection in a horizontal layer of binary fluid mixture heated from below is a paradigm for oscillatory pattern forming systems [1]. An important generalization of the conventional type of the problem is the convection with a lateral through-flow. This generalization provides the unique opportunity to study pattern formation in a system with broken left-right parity. The symmetry breaking caused by the throw-flow lifts degeneracy of the problem and for this reason must affect the pattern dynamics dramatically. Thus, study of this type of convection sheds a light on generic aspects of pattern formation in systems with broken parity, which attaches especial importance to the problem.

The linear stability analysis (LSA) of the spatially uniform conducting state performed in Ref. [2] reveals that the through-flow splits the single Hopf bifurcation point, corresponding to the convection threshold without the trough-flow, into two Hopf bifurcation points for upstream (UTW) and downstream (DTW) traveling waves, respectively. It is important that the values of the thresholds as well as their relative positions with respect to each other depend on the value of the Reynolds number (*Re*) for the through-flow. Nonlinear effects are studied numerically in recent publication [3], where a number of interesting results is obtained. However, the small value of aspect ratio employed in Ref. [3] does not allow the authors to answer the most appealing question "How does the trough-flow affect nonlinear stage of pattern formation and pattern selection in an extended channel, where the pattern structure is not imposed by the lateral boundary conditions?"

The first attempt to answer this question is made in the present Letter. To this end we perform numerical integration of the standard set of two-dimensional (one horizontal coordinate x and vertical coordinate z, where z-axis is antiparallel to the gravitational acceleration) hydrodynamic equations in the Oberbeck-Boussinesq approximation. The equations may be found, e.g., in Ref. [3] and are not written here explicitly. We employ the usual non-dimensional variables, where length is measured in units of the layer width d and time in units of heat diffusion time d^2/χ (here χ is the thermometric conductivity).

The aspect ratio Γ is chosen equal to 12. The boundary conditions at the upper and lower confining surfaces are rigid, isothermal and impermeable. The lateral boundary conditions for the temperature and concentration fields at the inlet ($x = 0$) yield the basic linear profiles, while at the outlet ($x = \Gamma$) we require vanishing of the corresponding x-derivatives. As for the lateral boundary conditions for the velocity field, they impose the same Poiseuille profile both at the inlet and outlet. These boundary conditions simulate the ones, which may be imposed in real experiment, cf., e.g., the boundary conditions for similar problems with a through-flow employed in Refs. [4,5]. In addition, suppression of the convection close to the in- and outlet allows us to minimize influence of the lateral boundaries on the pattern selection process. The latter has especial importance due to possibility of advection with the trough-flow perturbations generated by the inlet into the bulk of the channel.

The Prandtl number ($Pr \equiv \nu/\chi$, where ν stands for the kinematic viscosity) is chosen equal to 10, the Lewis number ($L \equiv D/\chi$, where D is the concentration diffusion coefficient) is 0.01. Such a choice of the constants corresponds to commonly used in experiment room temperature ethanol-water solution. For the separation ratio $\psi \equiv S_T C_0(1 - C_0)\beta/\alpha$, which is the measure of coupling between the temperature and the concentration gradients coursed by the Soret effect, the moderate value $\psi = -0.1$ is chosen. Here α and β are the thermal and solute expansion coefficients, S_T stands for the Soret coefficient and C_0 is the mean concentration of the solution. The role of control parameter plays the reduced Rayleigh number r, which at the fixed values of the material constants of the fluid, actually, equals $\Delta T/\Delta T_c$, where ΔT designates the temperature

difference between the bottom and the top of the layer and ΔT_c corresponds to the threshold of instability of the conductive state of the pure fluid without the through-flow ($Re = 0,\ \psi = 0$) against infinitesimal perturbations. In simulations discussed in the present Letter r varies in rather a narrow interval close to $r = 1.2$. The trough-flow runs along the positive direction of x-axis and remains the same in all the simulations. The corresponding Reynolds number is 0.08 [6]. At these r and *Re* the characteristic values of the velocity of the shear flow are about 15–20% of the amplitude of the saturated convection velocity, i.e., the through-flow is always weak.

The SIMPLE code [7] with 242×22 grid points and temporal step $5 \cdot 10^{-4}$ is employed for the integration. The simulation gives rise to the following results.

We begin with $r = 1.20$. This value of r lies close to the thresholds of instability of the conducting state against infinitesimal perturbations for both types of waves UTW and DTW [8]. The initial conditions are the conductive state with the temperature field perturbed by random noise with the amplitude about 10^{-4}.

The simulations show that initially the conductive state becomes unstable against both the types of the waves. The corresponding pattern consists of superimposed, counter-propagating UTW and DTW. At the discussed initial stage of the instability the profiles of hydrodynamic variables for each type of the waves obey the relations following from the LSA (we will name these waves *linear* waves), being proportional to

$$\exp[\gamma^{U,D} t + \mu^{U,D} x + i(k^{U,D} x - \omega^{U,D} t)], \tag{1}$$

and similar to those in binary mixture without the trough-flow [9]. Here the superscripts U and D stand for up- and downstream propagating waves and $\omega^U < 0,\ \mu^U < 0,\ \omega^D > 0,\ \mu^D > 0$. The wavenumbers for both types of the observed waves $k^{U,D} \approx 3.2$, are quite close to the values of the critical wavenumbers (the ones maximizing the real parts of the growth rates for UTW and DTW at the corresponding thresholds), given under the specified conditions by LSA [10]. As for $\omega^{U,D}$, the expression obtained in Ref. [2] says that in the case under consideration for both types of the waves

$$\omega_c^{U,D} \approx \pm 6.47 + 41.9 Re, \tag{2}$$

where $\omega_c^{U,D} \equiv \omega^{U,D}(k_c)$ at the instability threshold and signs plus and minus are related to down- and upstream waves respectively. The two terms in r.h.s. of Eq. (2) have clear physical meaning, the first (± 6.47) is associated with the Hopf bifurcation without the through-flow, while the second describes the drift-effect caused by the through-flow. The observed values of $\omega^{U,D}$ ($\omega^U \approx -3.32,\ \omega^D \approx 9.40$) also are in reasonable agreement with those given by the above expression ($\omega_c^U \approx -3.11,\ \omega^D \approx 9.82$).

However, the real part of the growth rate for UTW is bigger than that for DTW [2]. Accordingly, soon UTW overtake DTW and begin to suppress them. During this process the amplitude modulations caused by superposition of the two types of waves become weaker and weaker. Finally, DTW are suppressed completely and oscillatory growth of the amplitudes of convective modes is transformed into purely exponential. In other words, the system evolves to the state with the entire channel filled with UTW, who still obey Eq. (1). It happens at $t \approx 3.5$, when the maximal amplitude of the z-component of the velocity field is about 10^{-2}. Thus, the first nonlinear effect observed in the simulation is the suppression of DTW, which agrees with the results obtained in Ref. [3] for small aspect ratio.

Then, the growth of the amplitude of UTW brings about the next nonlinear effects, which change the evolution of UTW themselves. As usual [1], when the amplitude becomes big enough nonlinear stabilization occurs. The corresponding nonlinear terms affect both the real and imaginary parts of the growth rate. Thus, when the amplitude reaches the vicinity of its quasi-steady value, determined by the balance between linear instability and nonlinear stabilization, the frequency of UTW begins to increase sharply [the frequency for the linear UTW is *negative*, see Eq. (2), so the increase of the frequency means decrease of its absolute value]. It gives rise to slowing down of the phase velocity of the waves and finally to their reversion, see Fig. 1c.

In the left half of the channel the scenario is different due to influence of the convection-suppressing conditions drifted from the inlet with the trough-flow. Here the exponential growth of the waves' amplitude suddenly, before the amplitude achieves the quasi-steady value, is changed with sharp decay. The convection in this half of the channel is suppressed and the fluid returns practically to the conductive state. The case is somewhat similar to that for convection in pure fluid with through-flow, where highly nonlinear states may be observed only at a certain distance from the inlet [11,12].

Regarding the reversed waves, in the end of this stage they transform into a quasi-steady wave train with pronounced left boundary propagating to the outlet. However, actually these waves remain UTW, which are just drifted downstream due to advection with the trough-flow. The concentration mode for these waves is shifted about one-quarter wavelength to the *left* of the w mode, where w stands for z-component of the velocity field in the midplane, so that counterclockwise circulating rolls have higher concentration level than that for the clockwise, see Fig. 1d. Such a phase shift is typical to UTW, while for DTW the phase shift has the opposite sign. Another evidence of the UTW nature of these waves is their small phase velocity $v_{ph} \approx 0.43$, which is smaller than both the maximal velocity of the trough flow $v_{fl}^{max} = 1.20$ and its average velocity $\bar{v}_{fl} = 0.8$.

At small Reynolds numbers we can write $v_{ph}(r, Re) \approx v_{ph}(r, 0) + v'_{ph}(r, 0)Re$, where the second term in the r.h.s. of this expression may be regarded as the drift velocity of the pattern v_{dr}. Generally speaking, the value of v_{dr} should be different from both v_{fl}^{max} and $\bar{v}_{fl}$ due to the problem nonlinearity. To obtain v_{dr} the following approach is employed. For a given pattern we switch off the trough-flow (replacing the lateral boundary conditions for the velocity field with rigid, impermeable) and observe the dynamics of the same pattern but without the through-flow.

As soon as the trough-flow is switched off the described quasi-steady waves change the direction of propagation and begin to travel upstream with the phase velocity $v_{ph} \approx -0.56$, which yields v_{dr} the value $v_{dr} \approx 0.99$ very close to the drift velocity given by Eq. (2) for the linear waves. Bearing in mind all mentioned above, we will name these nonlinear quasi-steady waves drifted downstream *false downstream traveling waves* (FDTW).

Since DTW are suppressed, the reversion of the left marginal wave in the UTW wave train creates on xt-plane a region shielded for perturbations from past to enter. The conductive state in this "restricted area" is destroyed with growth of small perturbations generated by the boundary between this region and the one filled with FDTW. It gives rise to secondary linear UTW propagating from the boundary of the FDTW wave train to the inlet, whose profiles are well described by Eq. (1), see Fig. 1c.

One by one the FDTW reach the outlet and vanish there. It results in contraction of the domain filled with FDTW and expansion of the one filled with linear UTW, respectively. It could be expected that finally all FDTW disappear by the outlet but, actually, it is not the case. Suddenly the amplitudes of FDTW begin to decay very fast. The decay yields deceleration of FDTW in

the laboratory coordinate frame and eventually change the direction of their propagation, i.e., the inverse transformation from FDTW to UTW occurs. The entire channel becomes filled with linear UTW and then the cycle (UTW $\rightarrow$ UTW + FDTW $\rightarrow$ UTW) is repeated periodically with the period about 24 time units, see Fig. 1c. Possible qualitative explanation of this re-linearization of the convection may be as follows. The narrower the domain filled with FDTW the weaker its stability. When the left boundary of the wave train advances close enough to the outlet, the wave train cannot stand against convection-suppressing influence of the lateral boundary conditions, which eventually results in decrease of the waves' amplitude, i.e., to the re-linearization.

To examine how the described nonlinear evolution depends on the Rayleigh number the simulations are repeated at different values of r. However, under the specified conditions the bifurcation from the conductive to convective state in binary mixture is subcritical [1] and the dependence of pattern structure on the Rayleigh number must exhibit a hysteretic loop. In this case to avoid jumps to another branch of the bifurcation curve the patterns obtained as the asymptotic state at the previous value of r are employed as the initial conditions for the new values of r.

The simulations show that in the region from the lowest inspected value of $r = 1.16$ up to $r = 1.21$ the pattern formation basically corresponds to the scenario discussed above. The saturated amplitude of the quasi-steady waves and the corresponding frequency both occur monotonically increasing functions of r, see Figs. 1–2. The phase velocity of the quasi-steady waves vanishes at $r \approx 1.17$. Accordingly, FDTW do not exist at r smaller than this value, cf. Fig. 1a and b.

Since the effect of the sudden decay of convective modes definitely is connected with the convection-suppressing lateral boundary conditions, it becomes more pronounced with decrease of r resulting in general degradation of the convection. In accordance with that the width of the decay region increases, while the fraction of the period, when the quasi-steady nonlinear waves exist, decreases with decrease of r, cf. Fig. 1 c, b and a. Alternatively increase of r eventually eliminates the inverse transition FDTW $\rightarrow$ UTW at all, see Fig. 1e, f.

Increase of the Rayleigh number from $r = 1.21$ to $r = 1.213$ brings about a new bifurcation. FDTW are accelerated. Both the amplitude of FDTW and their phase velocity increase and finally the phase velocity becomes equal to $v_{ph} \approx 1.20$, which is ***bigger*** than the drift velocity, Fig. 1g. Thus, FDTW transforms into true DTW. The transformation is accompanied with the corresponding change of the phase shift between the concentration and w modes, so that now counterclockwise circulating rolls have smaller concentration level than that for the clockwise, see Fig. 1h. In the same time linear UTW in the left half of the channel do not undergo the sudden decay any more. Eventually the system evolves to a steady state with left part of the channel filled with the linear UTW, which obey Eq. (1), and right part with the nonlinear steady DTW. The boundary between these two domains remains practically immobile.

Another important feature of the problem revealed in simulations is strict wavenumber and frequency selection. Every value of the Rayleigh number yields a certain unique pair of k and ω for each of the discussed types of the waves. Any change of r triggers transient process, which results in the corresponding changes of k and ω. The dependence of k and ω on r for nonlinear quasi-steady UTW, FDTW and DTW is presented in Fig. 2. It is important to stress that the imposed boundary conditions prevent any phase pinning or wavenumber discretization, so the observed wavenumber selection is the generic, intrinsic feature of the problem, which is not related to any external factor.

Note that transition UTW $\rightarrow$ FDTW does not change the smoothness of curves $k(r)$ and $\omega(r)$, while transition FDTW $\rightarrow$ DTW does, see Fig. 2. An interesting feature of the phenomenon is

that the functions $k(r)$ and $\omega(r)$ for UTW and FDTW are much sharper than those for DTW, cf. the behavior of these function blow and beyond the transition point. At decrease of r a narrow hysteretic loop for inverse transition DTW $\rightarrow$ FDTW is observed. DTW remain stable until $r = 2.09$. Further decrease of the Rayleigh number to $r = 2.08$ triggers transformation DTW $\rightarrow$ FDTW with formation of a pattern similar to that shown in Fig. 1c.

The last issue to be discussed is the global stability of the observed waves. According to the results of Ref. [3] for an unbounded in the lateral dimension channel steady nonlinear UTW should be unstable at employed in our simulations values of $\psi = -0.1$, $Re = 0.08$ and *any* value of r. The stable patterns observed in our simulations do not contradict to this result because their stability may be associated with the size-effect at the moderate value of $\Gamma = 12$ used in the simulations. To elucidate this question simulations with bigger value of Γ are required. These simulations are under way and will be reported elsewhere.

This work was supported by the Grant-in-Aid for Scientific Research (No. 11837006) from the Ministry of Education, Culture, Sports, Science and Technology (Japan). Japanese Government Scholarship for one of us (G. D. Li) is gratefully acknowledged.

REFERENCES

[1] M.C.Cross, and P.C. Hohenberg, Rev. Mod. Phys. **65**, 851 (1993).

[2] Ch. Jung, M. Lücke, and P. Büchel, Phys. Rev. E **54**, 1510 (1996).

[3] P. Büchel and M. Lücke, Phys. Rev. E **61**, 3793 (2000).

[4] J. M. Luijkx, J. K. Platten, and J. C. Legros, Int. J. Heat Mass Transfer **24**, 1287 (1981).

[5] K. L. Babcock, G. Ahlers, and D. S. Cannell, Phys. Rev. E **50**, 3670 (1994).

[6] The characteristic value of the velocity of the trough-flow, which enters into the Reynolds number is that average over the Poiseuille profile.

[7] S. V. Patankar *Numerical Heat Transfer and Fluid Flow* McGraw-Hill, 1980.

[8] At the given values of the parameters the linear stability analysis for the infinitely-extended in x-direction layer yields the following thresholds $r^U \approx 1.12;\ r^D \approx 1.13$ [2]. In our simulations the thresholds should be a little beyond these numbers due to the finiteness of the aspect ratio and the stabilizing role of the lateral boundary conditions (*size-effect*). Thus, for r^U we obtain 1.155. As for r^D, it is much more difficult to obtain its value from the simulation due to the suppression of DTW by UTW (see further discussion in the text). However, the good agreement between r^U obtained in our our simulation and in Ref. [2] allows us to suppose that r^D in our case is also close to the corresponding value of Ref. [2].

[9] M. C. Cross, Phys. Rev. Lett. **57**, 2935 (1986).

[10] Precise quantitative comparison is difficult since dependence $k_c^{U,D}(Re)$ in Ref. [2] is given as a plot, where two branches $k_c^U(Re)$ and $k_c^D(Re)$ merge at $Re = 0$.

[11] H. W. Müller, and M. Lüke, Phys. Rev. A **45**, 3714 (1992).

[12] A. Couairon, and J. M. Chomaz, Phys. Rev. Lett. **79**, 2666 (1997).

FIGURES

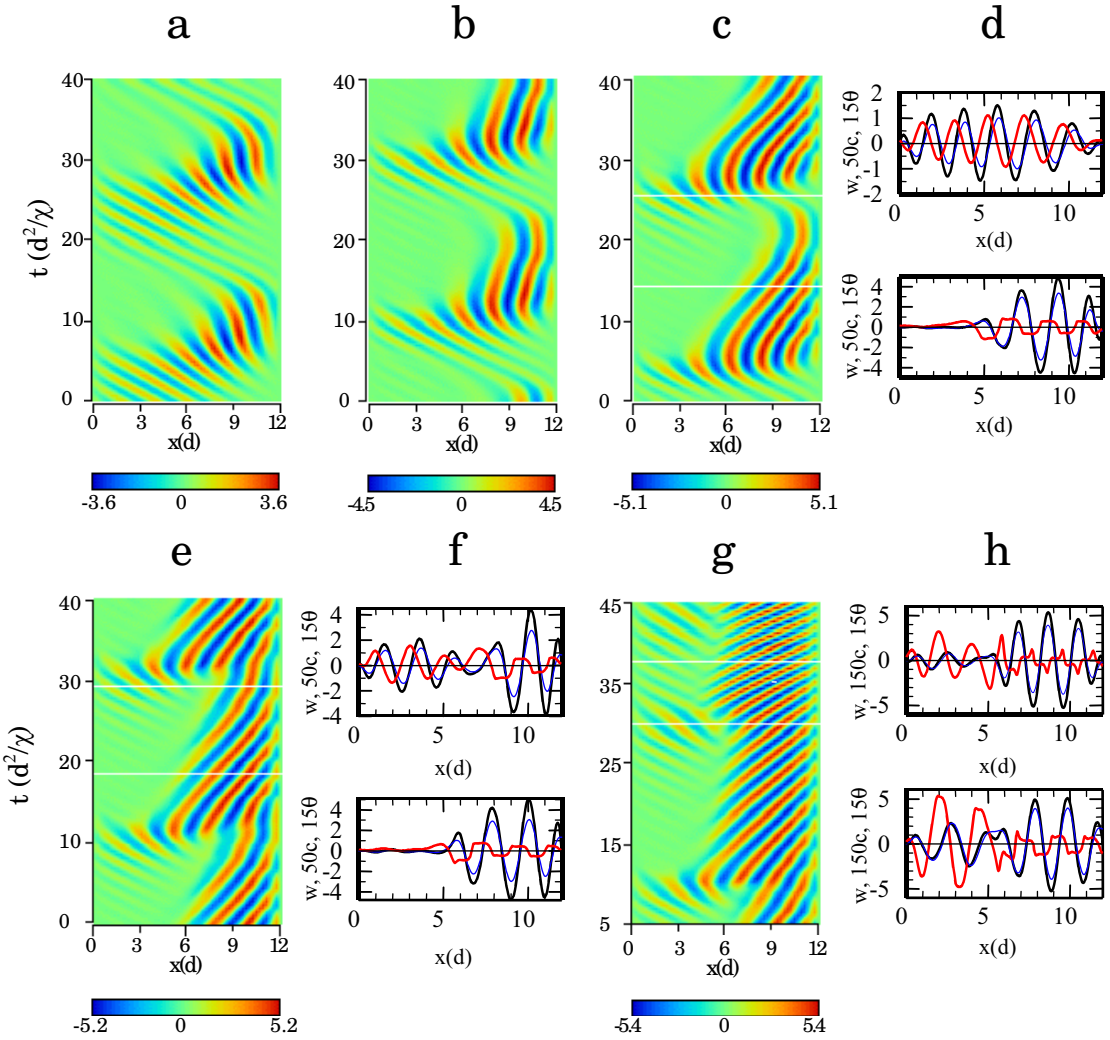

FIG. 1. Spatiotemporal plots for z-component of the velocity field in the midplane w at different values of the Rayleigh number and profiles of w (black), concentration $c \equiv (C - C_0)\beta/(\alpha\Delta T)$ (red) and temperature $\theta \equiv (T - T_0)/\Delta T$ (blue) fields in the midplane at some characteristic moments of time. a, b, c, e — asymptotic, periodically repeated in time patterns at $r = 1.16$ (a), $r = 1.18$ (b), $r = 1.20$ (c) and $r = 1.21$ (e), respectively. d — profiles of w, c and θ for spatiotemporal plot c at two moments of time indicated in c as white lines, the upper and lower panels on d correspond to the upper and lower lines on c. f — analogous profiles for e. g — transition FDTW $\rightarrow$ DTW initiated by abrupt raise of r from 1.21 to 1.213 at $t = 0$. h — profiles of w, c and θ for plot g. The profiles in the lower panel (the lower white line on g) correspond to FDTW, while those in the upper panel (the upper white line on g) already to DTW. For more details see the text.

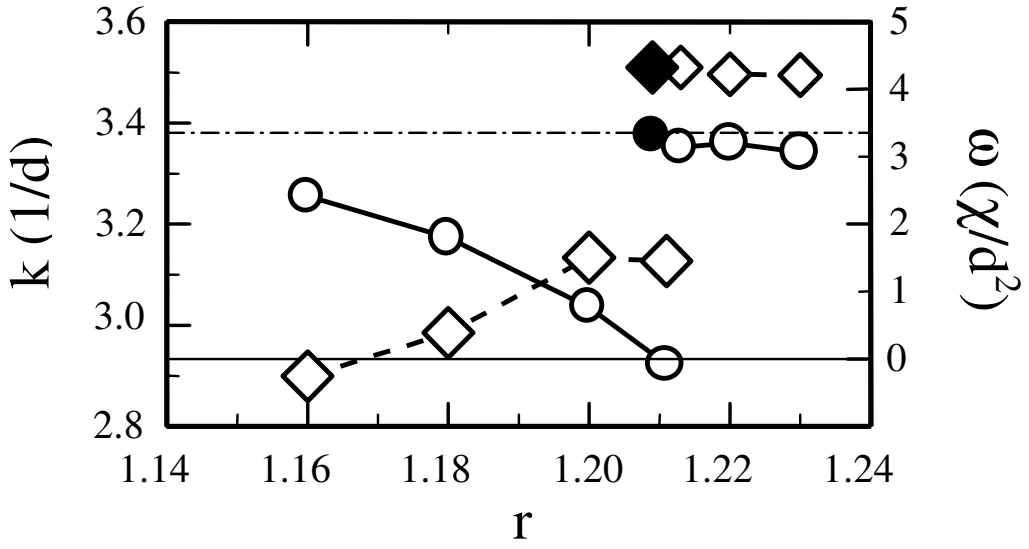

FIG. 2. The dependence of the wavenumber k ($\circ$) and oscillation frequency ω ($\diamond$) on the reduced Rayleigh number r for nonlinear quasi-steady UTW, FDTW and DTW. Note the discontinuity at $r = 1.213$ caused by transition FDTW $\rightarrow$ DTW. Closed symbols designate the boundary of a hysteretic loop observed during decrease of r. Full straight line in the plot corresponds to $\omega = 0$, dashed to the drift contribution of the through-flow for the linear waves [second term in the r.h.s. of Eq. (2)].